Interaction between the Annual and Interannual Variations in the Equatorial Pacific*

SHANG-PING XIE

Joint Institute for the Study of the Atmosphere and Ocean, University of Washington, Seattle, Washington

(Manuscript received 4 May 1994, in final form 18 October 1994)

ABSTRACT

The interaction between the annual and interannual variations is investigated by contrasting a pair of experiments with a general circulation model of the tropical Pacific Ocean. The atmospheric forcing applied to the model includes both annual and interannual components. The phase of the annual forcing is shifted one-half year in the two runs, which are otherwise identical. Significant differences are found in the sea surface temperature (SST) evolution between the two runs that have the same interannual forcing function. SST anomalies tend to be phase-locked to the solar calendar and to appear in the cold season. A SST variance function in response to interannual forcings with a random phase distribution is constructed, which has an annual cycle and reaches its maximum in the cold season as is observed. It is suggested that this seasonality of an ocean origin is amplified by the interaction with the atmosphere, leading to the observed phase-locking.

The phase-locking of the interannual cycle and the interannual variation of the annual cycle in SST are two manifestations of the interaction between the annual and interannual cycles. A simple conceptual model is proposed to explain these two features, in which strong interaction between the annual and interannual cycles occurs through the nonlinearity associated with the thermocline depth change and upwelling.

1. Introduction

El Niño/Southern Oscillation (ENSO) is the largest source of climatic variability in the instrument measurement records, having pronounced effects on the climate in the Tropics and extratropics (Bjerknes 1969; Wallace and Gutzler 1981; Lau and Nath 1994; among many others). Comparable to ENSO in amplitude, the seasonal cycle in sea surface temperature has a dominant period of one year in the eastern equatorial Pacific (Horel 1982; Mitchell and Wallace 1992). The genesis of this SST annual cycle is a puzzle considering that the solar forcing at the top of the atmosphere, which is the forcing for the seasonal cycle in most of the world, has virtually zero annual component. With a simple coupled ocean–atmosphere model, Xie (1994a) proposes that the annual cycle in the solar radiation in the off-equatorial regions, causing changes in the meridional wind, remotely forces a SST annual cycle if the intertropical convergence zone stays in the Northern Hemisphere. It is now widely accepted that ENSO is caused by the instability of the mean state of the ocean–atmosphere system in the Tropics (Philander et al. 1984; Hirst 1988; Wakata and Sarachik 1991). Equilibrated ENSO-like oscillations have been observed in various nonlinear coupled ocean–atmosphere models, with (Zebiak and Cane 1987; Battisti 1988) or without (Anderson and McCreary 1985; Schopf and Suarez 1988; Xie et al. 1989; Neelin 1990; Philander et al. 1989) an explicit seasonal cycle. This indicates that ENSO is an intrinsic oscillatory mode of the ocean–atmosphere system and exists independent of the seasonal cycle. On the other hand, ENSO has been known for a long time to be strongly modified by the seasonal cycle. As a manifestation, SST anomaly associated with ENSO tends to peak in a particular season, which is the boreal spring along the South American coast (Rasmusson and Carpenter 1982; Deser and Wallace 1987). This phase-locking of the interannual SST anomaly to a calendar season has important implications for the prediction of ENSO and its global impact. In a coupled ocean–atmosphere model that has successfully predicted ENSO for the last ten years, there is a distinctive seasonal cycle in its prediction skill. The prediction scores are satisfactory in most months of the year, but they decrease dramatically in the boreal spring (Cane et al. 1986; Webster and Yang 1992).

The phase-locking of the ENSO to the annual cycle suggests a significant interaction between the two. Their interaction is also underlined by the results reported by Zebiak and Cane (1987) that the inclusion of the seasonal cycle leads to irregularity in their model ENSO. Jin et al. (1994) and Tziperman et al. (1994) further identified a route for model ENSOs to go from a limit cycle to chaos, based on the general theory of

* Joint Institute for the Study of Atmosphere and Ocean Contribution Number 260.

Corresponding author address: Dr. Shang-Ping Xie, Graduate School of Environmental Earth Science, Hokkaido University, Sapporo 060, Japan.

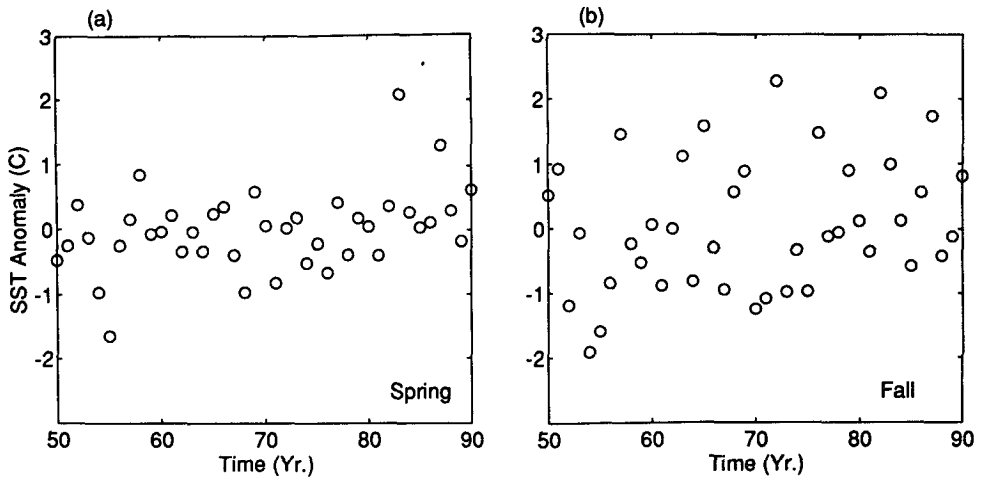

FIG. 1. Scatterplots of seasonal-mean anomalies of the COADS sea surface temperature as functions of time at 110°W on the equator for (a) Feb–Apr and (b) Aug–Oct.

a nonlinear oscillatory system. For oscillations with two distinctive frequencies such as the annual and interannual cycles to interact, we need to consider the nonlinearity of the system. Both the coupled ocean–atmosphere system and its two components are nonlinear. From these model studies and from observations, it is not clear whether the phase-locking of ENSO originates from the ocean or the atmosphere. Or does it arise only from the coupling between the two media? As a first step toward the understanding of the interaction between the annual and interannual cycle in the coupled system, we will only consider one of its components—the ocean—in this study. A state of the art ocean general circulation model (GCM) developed at the NOAA/Geophysical Fluid Dynamics Laboratory (GFDL) will be used. Forced with observed wind stresses and surface heat flux, this GCM has been used to make realistic simulations of both the seasonal cycle (Philander et al. 1987; Koeberle and Philander 1994) and ENSO (Philander and Seigel 1985; Rosati and Miyakoda 1988; Harrison et al. 1989). From these realistic simulations by the ocean GCM, however, it is hard to assess the importance of the seasonal cycle for ENSO since they only mimic one single realization of history on the earth.

The purpose of this study is to make a direct and explicit assessment of the impact of the seasonal cycle on the ENSO cycle in the context of the above mentioned ocean GCM. Sea surface temperature will be the focus of this study since it is the only oceanic variable that affects the atmosphere. The method we will use is to contrast the results of two experiments that are different only in the phase of annual forcing and are otherwise identical. We will see that there are significant differences in the interannual SST anomalies between the two model realizations of the ENSO cycle, although the interannual forcing is the same. Furthermore, the largest SST anomalies tend to be locked in phase with a calendar season as in the observations, although the forcing is not. It is hoped that by studying these idealized GCM experiments, we can identify nonlinear oceanic processes where strong interaction between the annual and interannual variations occurs. The annual cycle and ENSO share some of developmental characteristics, such as the cycle of the expansion and retreat of the equatorial cold tongue. They also have some fundamental differences, which will be discussed in the paper.

The rest of the paper is organized as follows: section 2 analyzes the Comprehensive Ocean–Atmosphere Data Set (COADS) and describes the phase-locking of the ENSO SST anomalies in the eastern equatorial Pacific; section 3 describes the model and experiment design; section 4 presents the results from the GCM experiments; section 5 proposes an explanation for these results; and section 6 is a summary of the paper.

2. Observed phase-locking

El Niño—the Christ Child in Spanish—was originally used to refer to the annual warmings at Christmas along the coast of South America, but now it more commonly means the abnormal warming at an interval of a few years. As the name reveals, the coastal warming associated with ENSO usually starts amplifying around Christmastime and peaks in the boreal spring (Rasmusson and Carpenter 1982; Deser and Wallace 1987). Since the ENSO warming on the coast coincides with the seasonal warming that also occurs in December through February, it is sometimes described as an amplification of the regular seasonal cycle.

The SST anomalies in the eastern equatorial Pacific far apart from the coast have a very different seasonal dependence. Figure 1 shows scatterplots of the SST

anomalies in the boreal spring and fall seasons at 110°W on the equator for the period 1950–1988 from the monthly COADS. The scattering around zero is generally small in boreal spring but large in other seasons, indicating that large SST anomalies are rarely observed in spring. During the 30-year period from the late 1950s to the early 1980s, no SST anomaly greater than 1°C is seen in the spring panel, whereas many points are outside of the 1°C boundaries in the fall panel. In the boreal fall season, the warm events generally have larger amplitude than the cold ones. Starting with the 1982–83 ENSO, some changes appear in the characteristics of warm ENSO events. The recent warm events exhibit large amplitudes in spring as well as in fall. It is interesting to note that the 1988 cold event is still phase-locked to the calendar; it peaks in the boreal fall but is not seen in spring. It is not clear what has caused the change in ENSO's phase since the 1980s. Long-term variations are a possible cause. For example, there seems to be a warming trend if one traces the cold extremes in Fig. 1b. In the presence of low-frequency variability, it is necessary to develop a method of extracting the interannual component.

The seasonal dependence of SST anomalies described above may be well summarized in Fig. 2, which depicts the standard deviation of the SST anomalies as a function of calendar month. There is an annual variation in the SST variance with a significant amplitude. The variance of SST is at its minimum in spring and its maximum in fall and early winter. The maximum variance is about twice as large as the minimum. The small amplitude of SST anomaly and the small signal to noise ratio may explain why the prediction skill decreases greatly in boreal spring in some dynamic prediction models of ENSO (Webster and Yang 1992).

The above analysis of COADS data shows that the largest SST anomalies in both warm and cold phases of ENSO tend to form in the cold (boreal fall) season of the regular annual cycle in the eastern equatorial Pacific. This phase-locking of the ENSO cycle to the seasonal cycle is certainly a result of the ocean–atmosphere interaction in the presence of the annual cycle. In the rest of the paper, however, we will focus on oceanic processes and see if a seasonal dependence arises in interannual SST anomalies without interaction with the atmosphere.

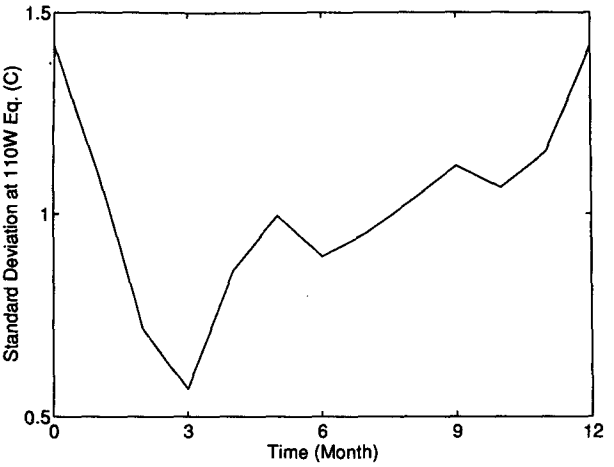

FIG. 2. Standard deviation of the COADS sea surface temperature anomaly at 110°W on the equator as a function of month.

3. Model and experiment design

The primitive equation GFDL Modular Ocean Model (MOM) was formulated by Bryan (1969) and documented by Pacanowski et al. (1990). The version we will use is very similar to that in Philander and Seigel (1985). Temperature is the only tracer explicitly calculated and salinity is fixed at 35 psu in the model. A surface heat flux package described in Rosati and Miyakoda (1988) is used. The solar radiation is absorbed at the surface and has a seasonal cycle given by Reed (1977). Vertical viscosity and diffusivity are calculated using a Richardson number–dependent scheme (Pacanowski and Philander 1981). Horizontal viscosity and diffusivity are 4×10^3 and 2×10^3 m^2 s^{-1}, respectively. The model has a flat bottom at 3000 m and 15 vertical levels with the first nine levels above 300 m to give high resolution in the upper ocean, the region in which we are especially interested. The zonal and meridional resolution is uniformly 3 deg and 1 deg, respectively. The model has a realistic coastal geometry and extends from 40°S to 40°N and from 130°E to 80°W. In the sponge layer poleward of 30°, Newtonian cooling is applied to relax the ocean temperature to the observed Levitus (1982) data. The implicit Coriolis force and the implicit vertical mixing schemes are turned on, and a time step of three hours is used.

For the purpose of this study, it is desirable to simulate the annual cycle as realistically as possible, a rather challenging task for the GCM. With only the wind forcing, the GCM annual cycle in SST is too weak and too confined to the east (Philander et al. 1987; Harrison 1991). Specifying the annual cycle in surface air temperature improves the simulation (Gordon and Corry 1991; Giese and Cayan 1993; Koeberle and Philander 1994). Several test runs are made and compared. An imposed surface air temperature field $T_a = T_a^{\text{coads}} + 1.5\tilde{T}_a^{\text{coads}} \exp[-(\varphi/3)^2]$, with its seasonal cycle enhanced at the equator as compared to observations, is found to give the best SST simulation. The resultant model annual cycle in SST has realistic amplitude, phase, and zonal extent at the equator (see the next section and Fig. 4a). Here φ is the latitude in degrees, T_a^{coads} is the monthly COADS climatology of surface air temperature, and $\tilde{T}_a^{\text{coads}}$ is the deviation from the annual mean. Because the heat content of the upper ocean is much larger than that of the atmosphere, the surface air temperature is to a large extent determined

by the sea surface temperature in the Tropics, rather than the other way around. Therefore, a simulation that imposes T_a may not be suitable for studying the genesis of the annual cycle in SST. Such a simulation, however, seems sufficient for the purpose of this study, which is to investigate the interaction between the annual and ENSO cycles rather than the genesis of the annual cycle itself. For the latter purpose, results from simple ocean (Seager et al. 1988) and coupled ocean–atmosphere (Xie 1994a) models are suggestive. Forced with the COADS monthly climatological wind and surface air temperature, the GCM is spun up for five years from the Levitus temperature field at rest. After the first two years, the model temperature and flow fields undergo steady seasonal cycles. The model SST field in the fifth year is saved and used to construct a field of air–sea surface temperature difference ($\Delta T = T - T_a$) together with the COADS air temperature field.

In the following experiments, the surface forcing to the ocean model consists of independent annual and interannual components. The annual forcings include the air–sea surface temperature difference ΔT constructed from the spinup run and monthly COADS climatological winds. Both of the annual forcings vary seasonally. In the Tropics the change in the surface air temperature generally follows that in SST. Therefore it is more appropriate to impose the air–sea temperature difference than the air temperature. The surface heat flux and the latent heat flux in particular act like a Newtonian cooling term in the SST equation. Imposing the air–sea temperature difference decreases the coefficient of this Newtonian cooling by a factor of four compared to the case of imposing air temperature if the relative humidity is 80% (Xie 1994b). This realistic small damping allows for large-amplitude interannual SST anomalies.

Our interannual forcing consists of only the zonal wind stress. The zonal wind anomalies associated with ENSO are observed to be largest around the date line and at the equator, decreasing away from the equator (Rasmusson and Carpenter 1982). The meridional wind anomalies show a less organized pattern near the equator. Based on these observed characteristics of wind anomalies, we use an analytical function form for our interannual wind forcing

$$u_{\mathrm{ENSO}} = \sin\left(\frac{\omega}{4}t\right)\left(\tanh\frac{\lambda-\lambda_1}{\Delta\lambda} - \tanh\frac{\lambda-\lambda_2}{\Delta\lambda}\right) \times \exp\left[-\left(\frac{\varphi}{9}\right)^2\right], \quad (3.1)$$

$$v_{\mathrm{ENSO}} = 0, \quad (3.2)$$

where ω is the angular frequency with a period of one year, λ is the longitude in degrees, $\lambda_1 = 150°$, $\lambda_2 = 220°$, and $\Delta\lambda = 10°$. As a result, the interannual forcing has a period of four years and repeats itself every four years. The amplitude of the zonal wind forcing is uniformly 2.0 m s^{-1} between 160°E and 150°W ($\lambda_2 = 210°$) at the equator and decreases rapidly away from this zonal extent. Experiments with a more complicated ENSO composite of observed winds, which includes many small time–space-scale features, yield very similar results to what we will describe.

We have conducted a set of experiments using the ocean GCM. In these experiments, the interannual forcing is kept the same. The phase of the annual forcing $F(t)$, however, is shifted by Δt months from that of the original forcing derived from the COADS, $f_{\mathrm{coads}}(t)$. In other words, the annual forcing $F(t) = f_{\mathrm{coads}}(t + \Delta t)$ is used instead of $f_{\mathrm{coads}}(t)$. Here annual forcing includes both wind and surface thermal forcings. The only difference among these experiments with various values of Δt is thus in the relative phase between the annual and interannual forcings. If the system is linear or the interaction between the annual and interannual cycles is weak, the SST anomalies from the mean annual cycle should be identical in these experiments. By comparing the SST anomalies in these experiments, we can assess the effect of the annual cycle on the interannual one. Starting from the appropriate month in the fifth year of the spinup run described above, the model is integrated for eight years (two cycles of the interannual forcing). The output from the second 4-yr cycle will be analyzed in the following section. The third cycle is found to be almost identical with the second in the extended experiments.

4. Results

We first focus on two experiments: one with $\Delta t = 0$ and the other with $\Delta t = 6$ months. As a result, the annual cycles in the two cases are 180° out of phase. In the $\Delta t = 6$ experiment, the sun is over the Tropic of Cancer in December and over the Tropic of Capricorn in June. The seasonal equatorial warming and cooling in the eastern Pacific occur in September and March, respectively, in contrast to the $\Delta t = 0$ case where they occur in March and September as in the observations.

Figure 3 depicts the mean state of the model at the surface for the $\Delta t = 0$ experiment, which resembles the observations in several aspects. A tongue of cold water extends westward along the equator into the central Pacific from the South American coast, caused by strong equatorial upwelling and intense vertical mixing. There is a warm water pool in the western equatorial Pacific, which extends eastward off the equator. The northern branch of the extension of warm water, reaching Central America across the basin, is considered to maintain the intertropical convergence zone in the Northern Hemisphere through ocean–atmosphere interaction (Xie and Philander 1994). All three major surface currents in the tropical Pacific—South Equatorial Current, North Equatorial Countercurrent, and

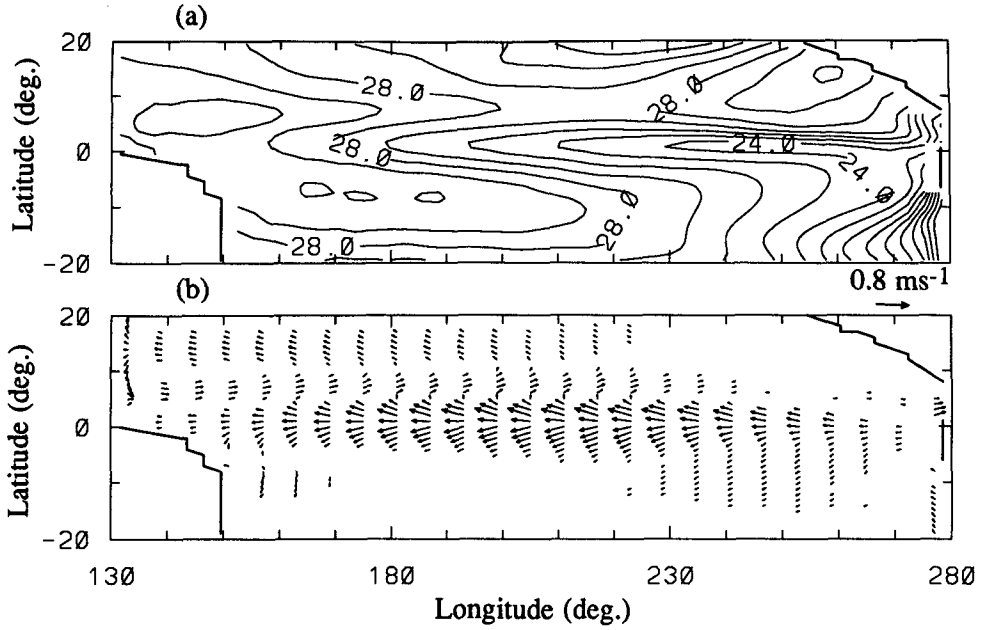

FIG. 3. Four-year mean fields of (a) sea surface temperature (contour interval: 1°C) and (b) surface current vectors in the ocean general circulation model.

North Equatorial Current—are present in the model simulation (Fig. 3b).

Figure 4a shows the time–longitude section along the equator for the $\Delta t = 0$ experiment of the climatological SST; this is obtained by averaging over an interannual cycle. The annual cycle has large amplitudes in the eastern Pacific and extends well into the central Pacific up to the date line. The surface water in these regions warms up in February through April and cools down in August through October. In the western Pacific, a weak semiannual cycle in SST exists, directly forced by that in the solar radiation. The amplitude, phase, and zonal extent of the equatorial seasonal cycle in this model simulation resemble to a large degree those observed in the real world (Mitchell and Wallace 1992). There is some indication of the westward propagation of the annual signals, but it is too weak compared to the observations. Figure 4b exhibits the time–longitude section of the temperature averaged from the surface to 300-m depth. This vertical-mean temperature is proportional to the dynamic height at the surface relative to the 300-m depth and an indication of the depth of the thermocline. When it is interpreted as a proxy to the sea level, effects of SST variations, as caused by zonal advection in the central Pacific, should sometimes be considered (Kawabe 1994). The change in the vertical-mean temperature is small on the annual timescale. It is roughly in phase with SST in the eastern Pacific but is out of phase in the central Pacific.

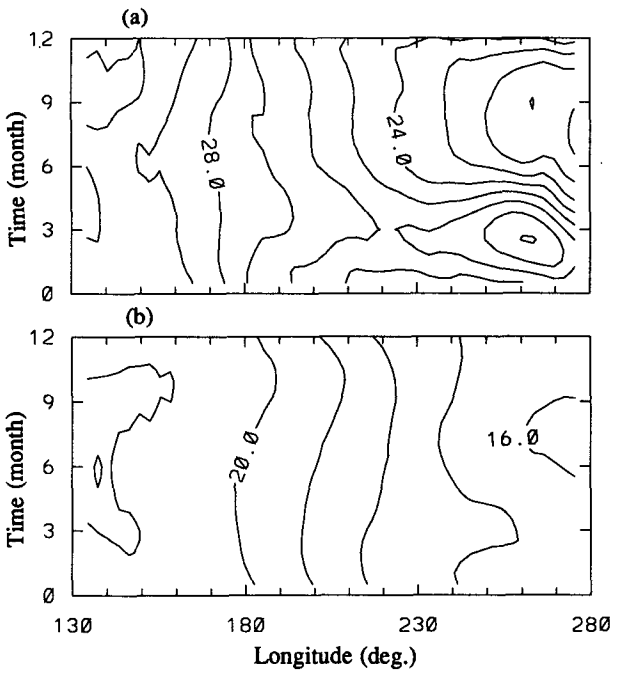

FIG. 4. Time–longitude sections of (a) sea surface temperature and (b) vertical-mean temperature from the surface to 300-m depth at the equator. These are obtained by averaging over a four-year interannual cycle and represent the time-mean annual cycle of the model.

Figure 5 depicts the time–longitude sections of the SST anomaly for the $\Delta t = 0$ case. Here and in the rest of the paper we will use the term "anomaly" to refer to the deviation from the mean seasonal cycle. Although the wind anomaly virtually vanishes in the eastern Pacific, there are large SST and vertical-mean

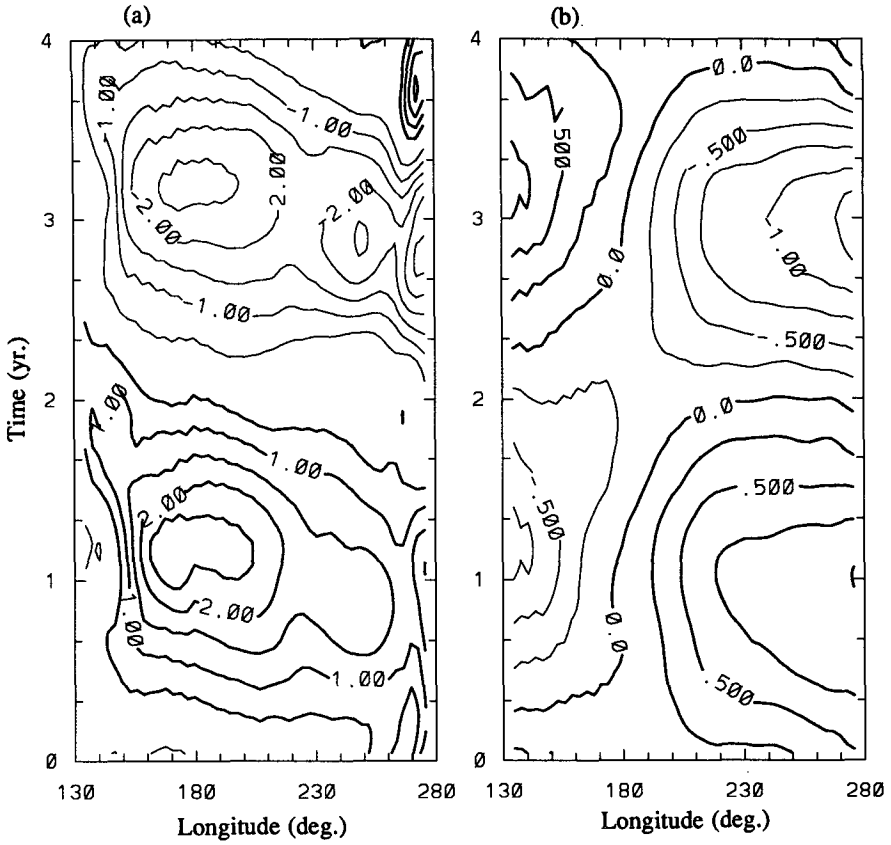

FIG. 5. Time–longitude sections of (a) sea surface temperature and (b) vertical-mean temperature anomalies at the equator (positive in bold and negative in thin lines), which are deviations from the mean annual cycle in Fig. 4. A 13-point running mean is applied to the twice monthly output. Contour intervals are 0.5°C with the zero contour omitted in (a) and 0.25°C in (b).

temperature anomalies, suggesting that these anomalies are remotely forced by the forcing in the central Pacific. The vertical-mean temperature anomalies are stationary and vary in a seesaw manner between the east and west. This stationary seesaw pattern is observed in the sea level observations (Wyrtki 1985) and in previous ENSO simulations (Busalacchi et al. 1983; Chao and Philander 1993). It is clear from the comparison between Figs. 4b and 5b that the interannual cycle in the vertical-mean temperature has a much larger amplitude than the annual one, suggesting that ocean dynamics play an important role in exciting the interannual variability. The SST anomaly has the largest amplitude at the date line, in contrast to the observed ENSO which decays from the eastern to the central Pacific. Unrealistically large SST anomalies in the central ocean are also reported in other GCM simulations (Philander and Seigel 1985; Rosati and Miyakoda 1988) and in coupled ocean–atmosphere models with the MOM as its oceanic component (Neelin 1990; Philander et al. 1989). Because of the poor simulation in the central and western Pacific, we will concentrate on the eastern Pacific, where the SST simulation is reasonably good.

Figure 6a shows the time–depth section of temperature at 110°W on the equator, which is characteristic of the eastern Pacific. The annual cycle can be clearly seen over the 4-year period. The seasonal warming in spring is associated with the increase in stratification, while the cooling in fall is associated with the destratification of the upper 50-m water column. The SST variation associated with the ENSO cycle is most clear by tracking the SST in the fall seasons: the SST in the fall of year 1 is above 24°C, while it is only 20°C in the fall of year 3. On the interannual timescale, there is a significant vertical displacement of the thermocline. In order to separate the annual and interannual components of the temperature deviation from the long-term annual mean, we first apply a 25-point running mean to the twice monthly model output to remove the annual cycle. The annual component is then obtained by subtracting the original data from the filtered ones. Figures 6b and 6c display the interannual and annual components, respectively. The annual cycle and ENSO share many similar features at the surface in the equatorial region; both are characterized by the development and decay of the equatorial cold tongue and by

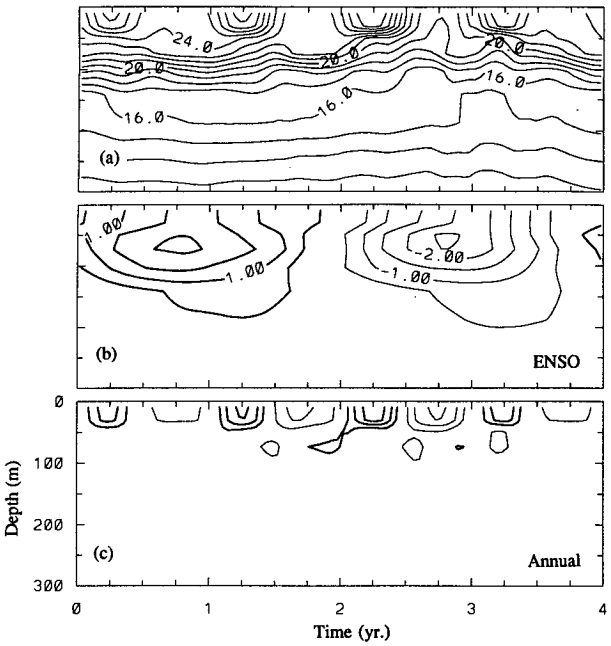

FIG. 6. Time–depth sections of (a) ocean temperature, its variations associated with (b) the interannual and (c) annual cycles (positive in bold and negative in thin lines) at 110°W on the equator: (b) is obtained by applying a 23-point running mean to the deviation (twice monthly) from the long-term mean profile to remove the annual variation; (c) is the residual of the total deviation from (b). Contour intervals are 1°C in (a) and (c) and 0.5°C in (b).

the strengthening and weakening of the South Equatorial Current. The two modes of oscillation, however, have a striking difference in vertical structure. Although having significant amplitude at the surface, the interannual mode has the largest amplitude at the depth of the thermocline. Its phase is nearly uniform in the vertical direction; the surface warming is associated with the deepening of the thermocline and vice versa, supporting the parameterization of the ocean mixed layer dynamics proposed by Philander et al. (1984) and widely used in simple coupled ocean–atmosphere models (Hirst 1988; Wakata and Sarachik 1991; Neelin 1991). Significant amplitudes of the annual mode, on the other hand, are confined to the upper 50-m water. There is not a well-defined phase relation between the changes above and below the 50-m depth. The shallow vertical scale and the lack of variation in the thermocline depth suggest that the annual cycle is excited by such local surface forcings as heat flux (Koeberle and Philander 1994) and wind stirring associated with the seasonal cycle in the meridional wind (Xie 1994a). Note that the amplitude of the annual cycle varies on the interannual timescale, a manifestation of the ENSO's influence. This feature will be discussed in more detail in the next section.

Now we compare the $\Delta t = 0$ and $\Delta t = 6$ experiments. Figure 7 shows the vertical-mean and surface temperature anomalies as functions of time at 110°W on the equator. The timeseries of the vertical-mean temperature in the two cases are almost identical and the difference between the two is very small. The vertical displacement of the thermocline is nearly in phase of the change in the trade winds; the thermocline deepens for the first two years when the trades relax and shoals for the last two years when the trades strengthen. In response to the sinusoidal variation in the zonal wind, the deepening and shoaling of the thermocline are roughly symmetric and have similar amplitude. All these indicate that the dynamic response of the ocean is essentially linear and is affected little by the annual cycle. This is why models with linear ocean dynamics can give a quite good simulation of ENSO (Busalacchi et al. 1983; Zebiak and Cane 1987). The time evolution of SST anomaly, on the other hand, exhibits remarkable differences between the two cases, although the interannual wind anomalies are the same. The difference of the SST anomalies can be as large as 1°C, which is on the same order of the SST anomaly itself. The SST variation in the $\Delta t = 0$ case has a larger amplitude than that in $\Delta t = 6$ case, and both its warm and cold phases are single-peaked. In the $\Delta t = 6$ case, on the

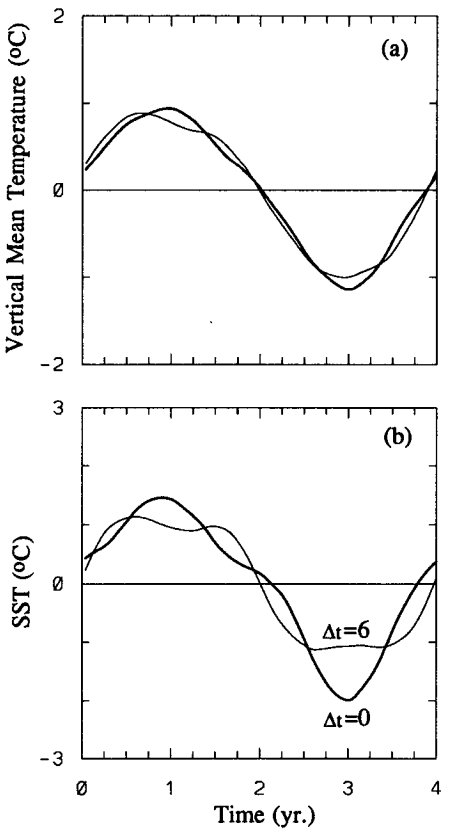

FIG. 7. Deviations from the mean annual cycle of the vertical-mean and sea surface temperatures as functions of time at 110°W on the equator. The thick lines are for the $\Delta t = 0$ experiment and the thin lines for the $\Delta t = 6$ experiment.

other hand, both the warm and cold phases of the interannual cycle in SST last for two years and have two peaks of comparable magnitude. The recent two El Niños, beginning in 1986 and 1991, have received much attention because both lasted for a prolonged period of 2 years in contrast to the previous 10 El Niños. Our experiments suggest that the relative phase between the annual and interannual forcings might be a factor that contributes to these different time-evolution patterns of the SST anomaly. It is also interesting to note that although the wind change is sinusoidal in time, the SST response is far from sinusoidal. In the $\Delta t = 6$ case, the transition from the warm to the cold phase takes less than a year, instead of two years as one might expect from the sinusoidal forcing function or the thermocline depth variation.

Another interesting feature of the SST anomaly evolution is that it peaks in the cold season of the annual cycle. In the $\Delta t = 0$ case, the positive and negative SST anomalies reach maxima in October of year 1 and in December of year 3, respectively, when the seasonal cooling occurs. In the $\Delta t = 6$ case, the SST anomaly tends to avoid these months to form its maxima when the seasonal warming occurs. Instead, it chooses the cold seasons before and after and has a double-peak feature as a result. The nonlinearity of the SST equation is such that in response to the same interannual forcing, largest SST anomalies tend to form in the cold season.

To see the seasonal dependence of SST anomalies in a more quantitative way, we plot in Fig. 8 the standard deviation of the SST anomaly at 110°W on the equator from a set of eight experiments with $\Delta t = 12n/8$ mo, $n = 0, 1, \cdots, 7$. Here we used the solar calendar as the horizontal axis and let the seasonal forcing have the same phase in these experiments. The phase of the interannual forcing is now shifted by 3/2 months from one experiment to the next, and the phase of the interannual forcing in these eight experiments is uniformly distributed in the interval of one year. There are $4 \times 8 = 32$ data points for each half month, and the standard deviations of these 32 data points is shown in the plot. There is a clear annual cycle in the SST variance. The variance is a minimum in June and reaches a maximum in October when the annual cycle in SST is in its cold phase. This variation of the variance of the interannual SST anomaly is consistent with the observed curve in Fig. 2 in the sense that both have an annual cycle. Differences in details are also evident; the minimum of the observed variance in spring is absent in the GCM, and the maximum variance in the GCM is two months too early compared to observations. We now consider the SST variance function in response to an infinite set of interannual forcing functions whose phase is random and has a white-noise distribution. By performing many experiments with $\Delta t = 12n/N$ mo, $n = 0, 1, \cdots, N-1$, we can obtain an approximation of the response variance function. We found that $N = 8$ is sufficient for this purpose;

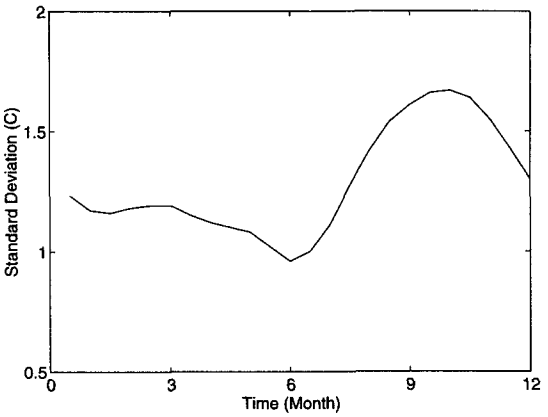

FIG. 8. Standard deviation of the model sea surface temperature anomaly at 110°W on the equator as a function of calendar month.

the variance function for $N = 8$ is nearly identical to those for two subsets of experiments with $\Delta t = 0, 3, 6, 9$ and $\Delta t = 1.5, 4.5, 7.5, 10.5$. It is thus suggested that even though the interannual forcing is random with a white-noise phase distribution, the interannual cycle in SST would still be phase-locked to the solar calendar and have its largest variance in the cold season.

5. Discussion

In a wavelet analysis of the COADS SST for the past 110 years, Gu and Philander (1995) found that the annual cycle in SST is modulated by the ENSO cycle; its amplitude increases in ENSO's cold phase but decreases in the warm phase. This can be seen in Fig. 6c as well; the annual cycle has the largest amplitude in year 3 when the annual-mean depth of the thermocline is at its minimum. Gu and Philander attribute this modulation of the amplitude of the annual cycle to the change in the upper-ocean heat content associated with ENSO. The coupled ocean–atmosphere is a highly nonlinear system in which the high-frequency and low-frequency oscillations can interact with each other. The amplitude modulation of the annual cycle represents the effects of the low-frequency ENSO on the high-frequency annual cycle. The phase-locking of ENSO, on the other hand, manifests the effects of the high-frequency annual cycle on the low-frequency ENSO. Here we propose an oceanic mechanism for these manifestations of the interaction between the two cycles.

The local oceanic processes are dominant and the horizontal advection of temperature seems to play a secondary role in causing the annual cycle in SST in the eastern Pacific (Hayes et al. 1991; Seager et al. 1988; Koeberle and Philander 1994; Xie 1994a). Let us consider a simple case where the annual cycle is directly

excited by the local change in surface heat flux,[1] that is,

$$\frac{\partial T_1}{\partial t} = \frac{Q_1}{H(1+h)}, \tag{5.1}$$

where T_1 is the annual variation of SST; $Q_1 = Q\cos\omega t$ is the annual surface heat flux forcing due to the annual cycle in cloudiness, wind speed, and hence surface evaporation; H is the annual-mean depth of the thermocline; h is the nondimensional perturbation in the thermocline depth scaled with H. In our GCM experiments, $h(\tau)$ is a periodic, sinelike function. Generally $h(\tau)$ can be of any functional form, periodic or not. Since the change in the thermocline depth is very small on the annual timescale (Fig. 6c), $h = h(\tau)$, where τ is the slow time that varies on interannual timescale. In the equatorial eastern Pacific, the change in the mixed layer depth follows that in the thermocline depth. In the warm phase of ENSO, for example, both the mixed layer and thermocline deepen. Here we assume that $h \ll 1$, which is true in our simulations (Fig. 6a) but may not be valid for strong ENSO events such as the 1982–83 ENSO. This assumption is purely for the convenience of discussion and does not qualitatively affect the conclusion. Under this assumption and because $o(t)/o(\tau) \ll 1$, one can linearize (5.1) with respect to h and obtain a solution to (5.1) under the WKBJ approximation

$$T_1 = A_1[1 - h(\tau)]\sin\omega t, \tag{5.2}$$

where $A_1 = Q/(\omega H)$ is the long-term mean amplitude of the annual cycle. In (5.2), the amplitude of the annual cycle, $A[1 - h(\tau)]$, is modified by the change in $h(\tau)$; it increases as the thermocline becomes shallow and decreases with the deepening of the thermocline. Following Philander et al. (1984), we assume the interannual SST anomaly T_A is proportional to that in the thermocline depth; that is,

$$T_A = \alpha h(\tau). \tag{5.3}$$

Although very crude, this parameterization is consistent with our GCM experiments (Fig. 6b). In the real ocean, however, the thermocline depth anomaly may lead SST anomaly by a few months (Kawabe 1994). The interannual climatic anomaly T', which is defined as the deviation from the mean annual cycle $\bar{T}_1 = A_1\sin\omega t$, is then

$$T' = (T_1 + T_A) - \bar{T}_1 = (\alpha - A_1\sin\omega t)h(\tau), \tag{5.4}$$

where T' is not only a function of the slow time τ but also of the fast time t. The amplitude of the interannual anomaly, $\alpha - A_1\sin\omega t$, is largest in the cold season when $\sin\omega t = -1$ and is smallest in the warm season when $\sin\omega t = 1$.

Figure 9 gives a schematic illustration of this phase-locking mechanism. In response to the interannual variation in the thermocline depth (Fig. 9a), the annual cycle amplifies in the cold phase of the interannual cycle but weakens in the warm phase (Fig. 9b). The total deviation of the SST from its long-term mean value is shown in solid line and the long-term mean annual cycle is in dashed line in Fig. 9c. The difference between the total deviation and mean annual cycle is plotted in Fig. 9d, which, regardless its sign, amplifies

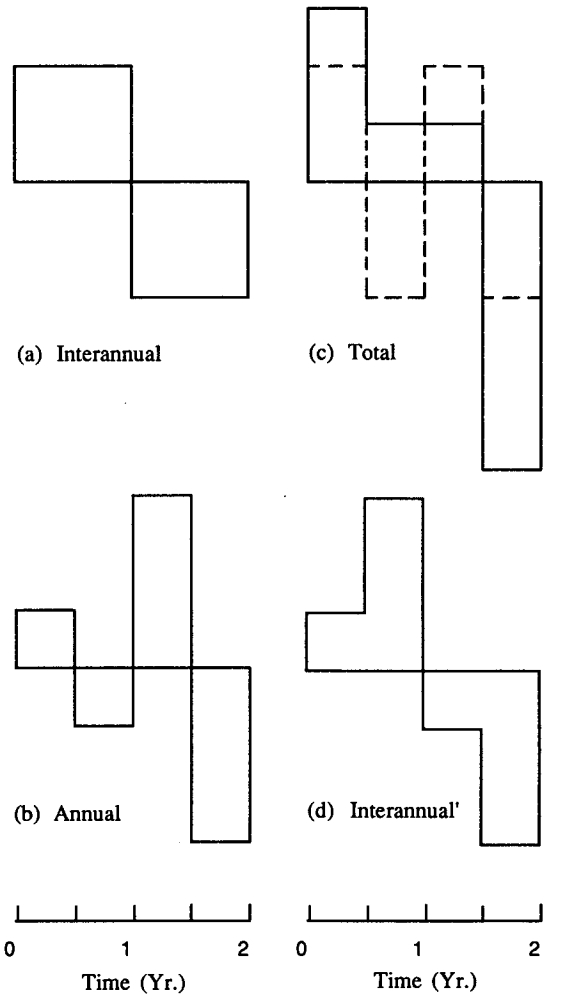

FIG. 9. Schematic illustrating how interannual anomalies of sea surface temperature are phase-locked to calendar seasons. (a) Interannual cycle in sea surface temperature or the thermocline depth, (b) annual cycle whose amplitude is modified by the interannual variation in the thermocline depth, (c) total SST deviation from the long-term annual-mean value and mean annual cycle (dashed line), and (d) SST deviation from the mean annual cycle.

[1] Other responsible local processes include the vertical mixing (Xie 1994a) and upwelling at the bottom of the frictional surface layer (Seager et al. 1994). A more general form of (5.1) is $\partial T/\partial t = A(h)e^{i\omega t} - d(h)T_1$, where A is the forcing amplitude and d is the damping rate, both of which can be modified by the interannual change in the thermocline depth. The argument in this section holds for this more general case, although a more complicated relation between the amplitude and $h(\tau)$ may arise.

in the cold season, although the original interannual cycle in Fig. 9a has no seasonal dependence.

In this simple model, the effect of the interannual cycle on the amplitude of the annual cycle can cause the interannual cycle in SST to be locked in phase with the solar calendar. Key to this argument is that the annual cycle in SST does not repeat itself every year but changes in response to the interannual cycle. To study climate change, we need to define a normal climate, which is the long-term mean annual cycle. Since we are concerned about the change from this reference state of our climate, the varying part of the annual cycle is projected to the climatic anomaly, causing the phase-locking of the anomaly. This oceanic mechanism for SST phase-locking does not require a seasonal dependence of $h(\tau)$. It explains the annual cycle in SST variance in our GCM experiments where the interannual forcing and $h(\tau)$ do not have a preferred season. In a fully coupled ocean–atmosphere system, $h(\tau)$ may develop its own seasonal dependence as a result of its interaction with the atmosphere and the seasonal cycle. In such a case, ocean–atmosphere coupling is also responsible for SST phase-locking besides the proposed oceanic mechanism.

6. Conclusions

This study investigates the interaction between the annual cycle and ENSO and its consequences by using the COADS data, a simple mixed layer model, and an ocean general circulation model. The forcing applied to the GCM includes both the annual and an idealized interannual components. Although sharing several developmental characteristics in SST and surface current fields, the annual cycle and ENSO have very distinct vertical structures. ENSO has a deep vertical structure and involves the vertical movement of the thermocline, whereas the annual cycle is shallow and confined to the top 50-m depth. This difference in the vertical structure is observed in the eastern Pacific and has an important implication for the genesis of the annual cycle and ENSO (Xie 1994a). This study focuses on the comparison of two GCM experiments, which are identical except for a phase difference of one-half year in the annual forcing between the two. As expected, the vertical-mean temperature, a proxy of the thermocline depth and a dynamic variable, is nearly identical in the two experiments. In response to the same interannual wind anomalies, on the other hand, the SST anomalies show substantial differences both in phase and magnitude between the two experiments. The largest SST anomalies tend to form in the cold season of the annual cycle in the eastern Pacific. The model SST variance distribution as a function of calendar month exhibits an annual cycle similar to the observed variance distribution, suggesting that even if the interannual atmospheric forcing does not have any seasonal dependence and is random in phase, the interannual variation in SST can still be phase-locked to the calendar. Since there is no explicit feedback from the atmosphere in these ocean GCM simulations, this seasonality of SST anomaly on the interannual timescale is solely due to the nonlinearity of the ocean.

The phase-locking of ENSO SST anomaly and the amplitude variation of the annual cycle in SST are two observed manifestations of the interaction between the annual cycle and ENSO. A simple ocean mixed layer model is proposed that explains these two manifestations present in our GCM experiments under idealized forcing conditions. In this simple model, interannual variation in the thermocline depth changes the thermal inertia of the upper ocean and modifies the oceanic response to the annual forcing. The phase-locking of the interannual SST anomalies, on the other hand, arises as a result of our definition of climatic anomaly as the deviation from the long-term mean annual cycle. This phase-locking mechanism underlines the importance of correctly simulating the annual cycle for a successful simulation of the ENSO. Similar simulations with oceanic models intermediate between the simple model and GCM are useful for further testing this mechanism.

The significance of the annual cycle is revealed by another time-evolution characteristic of the simulated ENSO. In observations, a typical ENSO event lasts for only one year, but in some ENSO events, large SST anomalies can persist for two years. Both one-year and two-year ENSO events appear in our ocean GCM (Fig. 7b). In the model simulations, this difference in time evolution is caused by a phase difference between the annual and interannual atmospheric forcings. In addition to its effects on the ENSO in the Tropics, the seasonal cycle is also a key to how ENSO affects the climate in the extratropics. The organized Pacific–North American teleconnection pattern, which establishes a connection between the Tropics and extratropics, prevails in winter (Wallace et al. 1993). Therefore, an accurate prediction of tropical climate in winter is presumably crucial for the prediction of the global climate.

It is not surprising that in an ocean GCM some differences in SST anomalies would arise in response to a phase change in the annual forcing, since the SST equation is known to be highly nonlinear. It is not so obvious, however, that these differences are organized and SST anomalies develop a seasonal dependence in the absence of feedbacks from the atmosphere, as the present study demonstrates. The interannual wind forcing, which is prescribed and assumed to have no seasonal dependence in this study, is caused by the interannual variations in SST in the real world (Rowntree 1972; Zebiak 1982; among many others). In a fully coupled system, the phase-locking described in this ocean-only study is subjected to interaction with the atmosphere. In addition to the phase, the interaction between the annual cycle and ENSO can also lead

to changes in ENSO's frequency. In the presence of seasonal forcing, ENSO can be locked in frequency with the annual cycle or become irregular in some coupled models (Zebiak and Cane 1987). Jin et al. (1994) and Tziperman et al. (1994) demonstrate this effect of the annual cycle on ENSO in a model where the only nonlinearities lie in the ocean, suggesting the responsible nonlinearity being of an oceanic origin. The present study points to the nonlinearity associated with the changes in the thermocline depth and equatorial upwelling, demonstrating that strong interaction occurs between the annual cycle and ENSO through this nonlinearity. This mechanism of the interaction between the annual cycle and ENSO presumably operates also in the coupled ocean–atmosphere system. The ocean–atmosphere coupling, however, will certainly modify and complicate the pictures drawn from this study under idealized conditions.

Acknowledgments. The author would like to thank Ed Sarachik and Mike Wallace for discussions and suggestions; David Battisti, Nate Mantua, and an anonymous referee for comments on the manuscript; Daifang Gu and George Philander for the access to their unpublished manuscript. This work was supported by a University of Washington/NOAA JISAO fellowship (Cooperative Agreement NA37RJ0198).

REFERENCES

Anderson, D. L. T., and J. P. McCreary, 1985: Slowly propagating disturbances in a coupled ocean–atmosphere model. *J. Atmos. Sci.*, **42,** 615–929.

Battisti, D. S., 1988: The dynamics and thermodynamics of a warming event in a coupled tropical atmosphere–ocean model. *J. Atmos. Sci.*, **45,** 2889–2919.

Bjerknes, J., 1969: Atmospheric teleconnections from the equatorial Pacific. *Mon. Wea. Rev.*, **97,** 163–172.

Bryan, K., 1969: A numerical method for the study of the circulation of the World Ocean. *J. Comput. Phys.*, **4,** 347–376.

Busalacchi, A. J., K. Takeuchi, and J. J. O'Brien, 1983: Interannual variability of the equatorial Pacific—revisited. *J. Geophys. Res.*, **88,** 7551–7562.

Cane, M. A., S. E. Zebiak, and S. C. Dolan, 1986: Experimental forecasts of El Niño. *Nature,* **321,** 827–832.

Chao, Y., and S. G. H. Philander, 1993: On the structure of the Southern Oscillation. *J. Climate,* **6,** 450–469.

Deser, C., and J. M. Wallace, 1987: El Niño and their relation to the Southern Oscillation: 1925–1986. *J. Geophys. Res.*, **92,** 14 189–14 196.

Giese, B. S., and D. R. Cayan, 1993: Surface heat flux parameterizations and tropical Pacific sea surface temperature simulations. *J. Geophys. Res.*, **98,** 6979–6989.

Gordon, C., and R. A. Corry, 1991: A model simulation of the seasonal cycle in the tropical Pacific Ocean using climatological and modeled surface forcing. *J. Geophys. Res.*, **96,** 847–864.

Gu, D., and S. G. H. Philander, 1995: Secular changes of annual and interannual variability in the tropics during the past century. *J. Climate,* **8,** 864–876.

Harrison, D. E., 1991: Equatorial sea surface temperature sensitivity to net surface heat flux: Some ocean circulation model results. *J. Climate,* **4,** 539–549.

——, W. S. Kessler, and B. S. Giese, 1989: Ocean circulation model hindcasts of the 1982–83 El Niño; thermal variability along the ship of opportunity tracks. *J. Phys. Oceanogr.*, **19,** 397–418.

Hayes, S. P., P. Chang, and M. J. McPhaden, 1991: Variability of the sea surface temperature in the eastern equatorial Pacific during 1986–1988. *J. Geophys. Res.*, **96,** 10 553–10 566.

Hirst, A. C., 1988: Unstable and damped equatorial modes in simple coupled ocean–atmosphere models. *J. Atmos. Sci.*, **45,** 830–852.

Horel, J. D., 1982: The annual cycle in the tropical Pacific atmosphere and ocean. *Mon. Wea. Rev.*, **110,** 1863–1878.

Jin, F.-F., D. Neelin, and M. Ghil, 1994: El Niño on the Devil's Staircase: Annual subharmonic steps to chaos. *Science,* **264,** 70–72.

Kawabe, M., 1994: Mechanism of interannual variations of equatorial sea level associated with El Niño. *J. Phys. Oceanogr.*, **24,** 979–993.

Koeberle, C., and S. G. H. Philander, 1994: On the processes that control seasonal variations of sea surface temperatures in the tropical ocean. *Tellus,* **46A,** 481–496.

Lau, N.-C., and M. J. Nath, 1994: A modeling study of the relative roles of tropical and extratropical SST anomalies in the variability of the global atmosphere–ocean system. *J. Climate,* **7,** 1184–1207.

Levitus, S., 1982: *Climatological Atlas of the World Ocean.* NOAA Prof. Paper No. 13, U.S. Govt. Printing Office, 173 pp.

Mitchell, T. P., and J. M. Wallace, 1992: The annual cycle in equatorial convection and sea surface temperature. *J. Climate,* **5,** 1140–1156.

Neelin, J. D., 1990: A hybrid coupled general circulation model for El Niño studies. *J. Atmos. Sci.*, **47,** 674–693.

——, 1991: The slow sea surface temperature mode and the fast-wave limit: Analytical theory for tropical interannual oscillations and experiments in a hybrid coupled model. *J. Atmos. Sci.*, **48,** 584–606.

Pacanowski, R. C., and S. G. H. Philander, 1981: Parameterization of vertical mixing in numerical models of tropical oceans. *J. Phys. Oceanogr.*, **11,** 1443–1451.

——, K. Dixon, and A. Rosati, 1990: GFDL modular ocean model. GFDL Ocean Group Tech. Rep. 2, GFDL/NOAA, Princeton, NJ, 46 pp.

Philander, S. G. H., and A. D. Seigel, 1985: Simulation of El Niño of 1982–1983. *Coupled Ocean–Atmosphere Models,* Vol. 40, J. C. J. Nihoul, Ed., Elsevier Oceanogr. Ser., Elsevier, 517–541.

——, T. Yamagata, and R. C. Pacanowski, 1984: Unstable air–sea interactions in the tropics. *J. Atmos. Sci.*, **41,** 604–613.

——, W. Hurlin, and A. D. Seigel, 1987: A model of the seasonal cycle in the tropical Pacific Ocean. *J. Phys. Oceanogr.*, **17,** 1986–2002.

——, N.-C. Lau, R. C. Pacanowski, and M. J. Nath, 1989: Two different simulations of Southern Oscillation and El Niño with coupled ocean–atmosphere general circulation models. *Phil. Trans. Roy. Soc. London,* **A329,** 167–178.

Rasmusson, E. M., and T. H. Carpenter, 1982: Variations in tropical sea surface temperature and surface wind fields associated with the Southern Oscillation/El Niño. *Mon. Wea. Rev.*, **110,** 354–384.

Reed, R. K., 1977: On estimating insolation over the ocean. *J. Phys. Oceanogr.*, **7,** 482–485.

Rosati, A., and K. Miyakoda, 1988: A general circulation model for the upper ocean simulation. *J. Phys. Oceanogr.*, **18,** 1601–1626.

Rowntree, P. R., 1972: The influence of tropical eastern Pacific Ocean temperature on the atmosphere. *Quart. J. Roy. Meteor. Soc.*, **98,** 290–321.

Schopf, P. S., and M. J. Suarez, 1988: Vacillations in a coupled ocean–atmosphere model. *J. Atmos. Sci.*, **45,** 549–566.

Seager, R., S. E. Zebiak, and M. Cane, 1988: A model of the tropical Pacific sea surface temperature climatology. *J. Geophys. Res.*, **93,** 1265–1280.

Tziperman, E., L. Stone, M. Cane, and H. Jarosh, 1994: El Niño chaos: Overlapping of resonances between the seasonal cycle

and the Pacific ocean–atmosphere oscillator. *Science,* **264,** 72–74.

Wakata, Y., and E. S. Sarachik, 1991: Unstable coupled atmosphere–ocean basin modes in the presence of a spatially varying basic state. *J. Atmos. Sci.,* **48,** 2060–2077.

Wallace, J. M., and D. S. Gutzler, 1981: Teleconnections in the geopotential height field during the Northern Hemisphere winter. *Mon. Wea. Rev.,* **109,** 784–812.

——, Y. Zhang, and K.-H. Lau, 1993: Structure and seasonality of interannual and interdecadal variability of the geopotential height and temperature fields in the Northern Hemisphere troposphere. *J. Climate,* **6,** 2063–2082.

Webster, P. J., and S. Yang, 1992: Monsoon and ENSO: Selectively interactive systems. *Quart. J. Roy. Meteor. Soc.,* **118,** 877–926.

Wyrtki, K., 1985: Water displacement in the Pacific and the genesis of El Niño cycles. *J. Geophys. Res.,* **90**(C4), 7129–7132.

Xie, S.-P., 1994a: On the genesis of equatorial annual cycle. *J. Climate,* **7,** 2008–2013.

——, 1994b: The maintenance of an equatorially asymmetric state in a hybrid coupled GCM. *J. Atmos. Sci.,* **51,** 2602–2612.

——, and S. G. H. Philander, 1994: A coupled ocean–atmosphere model of relevance to the ITCZ in the eastern Pacific. *Tellus,* **46A,** 340–350.

——, A. Kubokawa, and K. Hanawa, 1989: Oscillations with two feedback processes in a coupled ocean–atmosphere model. *J. Climate,* **2,** 946–964.

Zebiak, S. E., 1982: A simple atmosphere model of relevance to El Niño. *J. Atmos. Sci.,* **39,** 2017–2027.

——, and M. Cane, 1987: A model of El Niño–Southern Oscillation. *Mon. Wea. Rev.,* **115,** 2262–2278.